DOI: 10.1002/adma.200601999

Nanoscale Deposition of Single-Molecule Magnets onto SiO_2 Patterns**

By *Ramsés V. Martínez*, *Fernando García*, *Ricardo García*,* *Eugenio Coronado*,* *Alicia Forment-Aliaga*, *Francisco M. Romero*,* and *Sergio Tatay*

New approaches to the fabrication of planar devices based on materials by design are critical for the development of organic electronics.[1–4] Conventional nanolithography techniques[5] (top-down), as well as self-organization of functional elements that take up proper positions and shapes and establish connections with other components (bottom-up) have been applied.[6–9] These approaches make use of specific interactions between the components and the substrate, such as hydrophobicity/hydrophilicity, electrostatic forces, or protein recognition. Several scanning-probe-based nanolithographies,[10–12] printing-based methods,[13] and parallel approaches based on the transfer of nanoparticles from a stamp[5] are also being pursued.

The discovery that magnetic hysteresis can also arise from high-spin molecules with a significant magnetic anisotropy has prompted interest in dodecanuclear manganese complexes of the general formula $Mn_{12}O_{12}(RCOO)_{12}(H_2O)_{12}$.[14–17] Potential applications of Mn_{12} single-molecule magnets (SMMs) as bits for information storage or "qbits" for quantum computation[18] require methods for nanoscale-controlled positioning and/or manipulation of those molecules. In the search for suitable procedures to deposit SMMs onto different substrates, physical laser-based techniques have been applied.[19] Other "nonchemical" strategies include patterning of Mn_{12} aggregates by using stamp-assisted deposition. This method provides size and distance control on multiple length scales.[20] SMM particles have also been obtained from polycarbonate thin films containing Mn_{12} complexes after exposure to organic solvent vapors.[21] Another approach relies on the ligand-exchange reaction between a Mn_{12} species and a carboxy-terminated self-assembled monolayer (SAM) deposited on gold or silicon.[22] This strategy has afforded a self-organized assembly of SMMs with coherence domains of approximately 40 nm.[23] A third approach is based on the chemical functionalization of the peripheral ligands. In this context, isolated Mn_{12} complexes containing sulfur-based end groups have been grafted onto Au (111) surfaces.[24] Indirect and direct patterning of these molecules by using the microcontact printing method has recently been reported.[25] However, currently none of these methods allow the positioning of one or just a few SMMs into a predetermined nanoscale region of the surface.

Our contribution to the implementation of positioning SMMs onto different substrates is based on the electrostatic interactions between a positively charged Mn_{12} derivative and the surface of interest. With this aim, we have synthesized several Mn_{12} complexes with appended cationic tetraalkylammonium groups.[26] Recently, well-isolated SMMs have been obtained by depositing the polycationic compound $[Mn_{12}O_{12}(bet)_{16}(EtOH)_4]^{14+}$ (denoted by Mn_{12}bet, where bet is betaine) onto a gold surface modified with a negatively charged SAM.[27] In this Communication, we report a process for the transfer of SMMs from a macroscopic liquid solution into a predetermined nanoscale region of a silicon surface. This method allows the fabrication of nanostructures consisting of Mn_{12}bet on a silicon oxide template while the rest of the macroscopic surface remains free of molecules. Local oxidation was used to fabricate silicon oxide nanopatterns, either dots or stripes, over a Si (100) surface coated with a SAM. Their width ranged from 30 to 500 nm whereas the length could be modified from a few nanometers up to several micrometers. Nanoscale direct assembly arose from a combination of three factors: i) the strength of the attractive electrostatic interactions between the molecules and the local oxides; ii) the weak repulsive interaction between the molecules and the unpatterned surface; and iii) the size of the nanopattern.

Local oxidation nanolithography (LON) allows the fabrication of templates as well as a variety of electronic, optical, and mechanical nanoscale devices.[10,28–30] It is based on the spatial confinement of the oxidation reaction within a water meniscus formed between a nanometer-size protrusion, usually, although not exclusively, the tip of an atomic force microscope, and the sample surface.[31]

[*] Prof. R. García, R. V. Martínez, Dr. F. García
Instituto de Microelectrónica de Madrid, CSIC
Isaac Newton 8, 28760 Tres Cantos, Madrid (Spain)
E-mail: rgarcia@imm.cnm.csic.es
Prof. E. Coronado, Dr. F. M. Romero, Dr. A. Forment-Aliaga, S. Tatay
Instituto de Ciencia Molecular (ICMol), Universidad de Valencia
PO Box 22085, 46071 Valencia (Spain)
E-mail: eugenio.coronado@uv.es; fmrm@uv.es

[**] We thank Carmen Serra for XPS and ToF-SIMS measurements and Marta Tello and Fabio Biscarini for useful suggestions. This work was supported by the EU Integrated Project NAIMO (NMP4-CT-2004-500355), MRTN-CT-2003-504880 (QuEMolNa), and FP6-515767-2 (MagMaNet NoE). Financial support from the MEC (Spain) (MAT2004-03849 and MAT2003-02655) and Generalitat Valenciana is also acknowledged. Supporting Information is available online from Wiley InterScience or from the author.

ADVANCED MATERIALS

The process followed to position individual Mn_{12}bet molecules is presented schematically in Figure 1a–d. A clean silicon surface was functionalized by using a SAM (Fig. 1a) of 3-aminopropyltriethoxysilane (APTES). In the next step, a region of the surface was modified by local oxidation (Fig. 1b). A 20 μL drop of a sonicated 1μM Mn_{12}bet solution in CH_3CN was deposited on the substrate (Fig. 1c). Deposition times varied between 30 s and several minutes (see below). After deposition, the substrate was rinsed in CH_3CN for a few seconds and blown dry in N_2 (Fig. 1d).

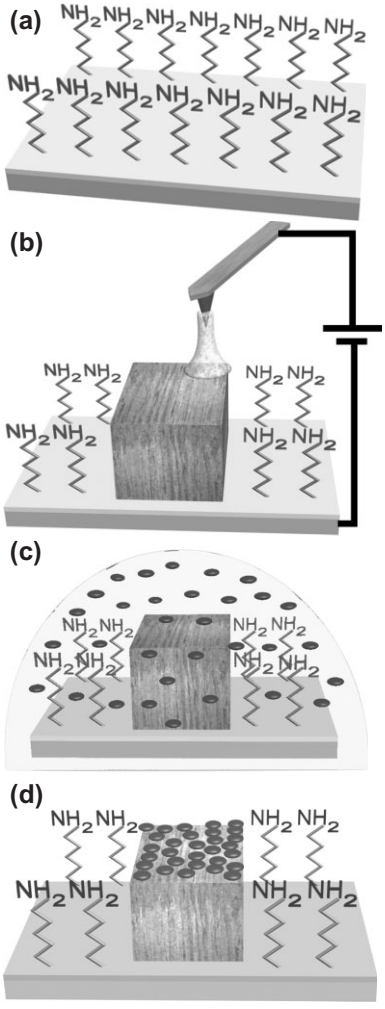

Figure 1. Schematic procedure of the nanoscale positioning of SMMs. a) Formation of an amino-terminated SAM on a Si (100) surface. b) Local oxidation of a region of the surface. c) Deposition of a macroscopic drop of a solution containing polycationic Mn_{12}bet (dark disks). d) Rinsing removes the molecules from the unpatterned areas. Polycationic Mn_{12}bet molecules are attached only to the nanopatterns.

Two parallel stripes nanofabricated by using LON are shown in Figure 2a. Each stripe consisted of 40 parallel lines 25 nm apart. Each line was about 3.2 μm long, 20 nm wide, and protruded 3.5 nm from the substrate baseline. Each oxide line was fabricated through the sequential application of a series of voltage pulses. Each voltage pulse (24 V, 10 ms) generated an oxide dot about 3 nm high (Fig. 2b) and 20–40 nm in diameter.[31] The resulting size depended on the tip–surface separation and meniscus size. Between pulses the tip was displaced laterally 5 nm.

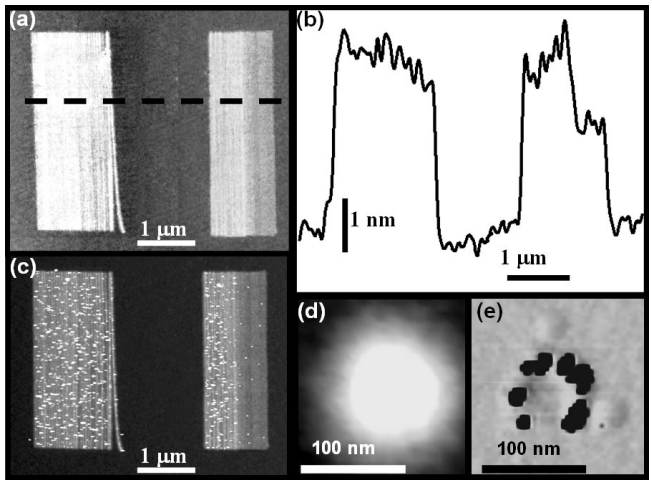

Figure 2. Patterns fabricated by using LON before and after deposition of SMM. a) An atomic force microscopy (AFM) image of two parallel stripes. b) A cross section along the line shown in (a). c) A topographic image of the pattern shown in (a) after the deposition of Mn_{12}bet. The SMM particles appear as white dots in the image. d) A topographic image of a local oxide dot 80 nm in diameter. e) The phase image reveals the presence of 16 SMM particles forming a nanoscale ring around the dot. The phase-shift image reveals the difference in mechanical properties between the molecules and the dot.

Figure 2c shows the local oxide nanopatterns from Figure 2a coated with Mn_{12}bet. Novel topographic features showing a disk-shaped morphology with an average height of 3.3 nm and an average width of 15 nm appear in the atomic force microscopy (AFM) image. These values differ notably from the molecular dimensions obtained from X-ray diffraction (XRD) data (1.6 nm × 2.2 nm), indicating the presence of molecular aggregates. Given that tip convolution effects produced images of the particles with an apparent diameter 2–5 times larger than their real value, we can safely postulate that the features contain a relatively small number of molecules (around 20).

To show that template growth of SMMs did not depend on the geometry of the nanopattern, we also patterned silicon oxide dots and repeated the aforementioned deposition process. Figure 2d shows an oxide dot of 80 nm diameter. Because dot and particle heights were comparable, SMMs were concealed by the topography. To distinguish substrate and nanopattern topographic features from the SMM morphology, we also performed dynamic force microscopy phase-contrast imaging. The sensitivity of phase imaging to changes in energy dissipation processes[32] enabled us i) to map topography separately from material properties and ii) to achieve compositional contrast at the nanoscale. The phase image revealed (Fig. 2e) that

16 particles (dark spots) were located preferentially around the dot edges. This gave rise to the formation of a nanoscale ring of SMMs. Previous reports have shown that rings of Mn_{12} SMMs can form spontaneously around water droplets on highly oriented pyrolytic graphite (HOPG) surfaces.[33] A similar phenomenon, based on adhesion forces, could be operative in this case.

The surface coverage in the left pattern of Figure 2c was ca. 300 particles μm^{-2}. Remarkably, there were no features outside the patterned area. This observation also applied to regions far from the patterned regions (from a distance of micrometers to millimeters). We attribute the source of the preferential interactions between Mn_{12}bet and the local oxide nanopatterns firstly to the attractive electrostatic interaction of the molecules with the trapped charges generated during the local oxidation process inside the oxide nanostructure,[34] and secondly, to the expected repulsive interaction between the amino-terminated monolayer and the positively charged polycationic derivative. To verify these hypotheses we used the neutral derivative $Mn_{12}O_{12}(CH_3COO)_{16}(H_2O)_4$ (denoted Mn_{12}Ac) as a blank in two different experiments. First, Mn_{12}Ac and Mn_{12}bet were deposited separately on two bare Si (100) substrates patterned with silica dots. After the substrates had been rinsed, we observed that the affinity of Mn_{12}bet for the local oxide dots was higher. This supports the fact that electrostatic interactions are important in the positioning process. In the second experiment, two APTES-modified Si (100) substrates patterned with silica dots were used to deposit Mn_{12}Ac and Mn_{12}bet separately. Interestingly, Mn_{12}Ac adhered both to the local oxide and the APTES-modified substrate with no selectivity, whereas the polycationic derivative was found almost exclusively in the patterned areas. This can be easily understood in terms of a repulsive interaction between the amino-terminated SAM and Mn_{12}bet, both of them being positively charged. The absence of molecules outside the patterned area emphasizes the extreme selectivity of this deposition process.

Finally, the dependence of Mn_{12}bet attachment on the density of the trapped charges within the local oxide was studied. For that purpose, we nanofabricated a rectangular stripe consisting of two regions with different heights, 3 nm and 2 nm from the bare substrate (right pattern of Fig. 2c). The height of the local oxide depends on the strength and duration of the applied voltage. The trapped charges, either buried or at the surface of the oxide, also depend on the total charge transfer between the electrolyte and the substrate, or, in other words, on the height of the oxide. After deposition and rinsing, the particles deposited on the taller section outnumbered those present in the short section by a factor of about six (in fact, 167:25). Furthermore, these experiments also indicated the characteristic length scale of the weakly screened long-range electrostatic forces generated by the trapped charges. By measuring the closest distance from the molecules deposited on the short section to the edge separating the two sections we estimated a characteristic electrostatic-interaction length of 40–50 nm.

The density of molecules deposited on a given nanopattern depended, for a fixed concentration, on the deposition time. Figure 3a and b show images of the same pattern after two successive depositions of 1 and 1 + 1 min, respectively. After each deposition, the sample was rinsed in the solvent for 15 s.

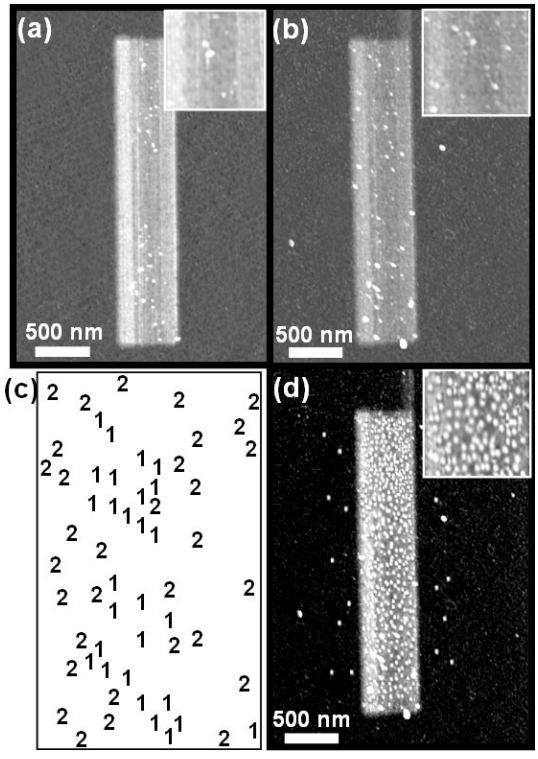

Figure 3. Time-dependent deposition studies. a) An AFM image of the patterned surface after 1 min deposition time. b) After 2 min deposition (1 + 1 min). c) A map of the local oxide stripe showing the molecules deposited after 1 min (labeled 1) and 2 min (labeled 2). d) AFM image of the same pattern after 4 min deposition (1 + 1 + 1 + 1 min). The insets show a magnified image of the uppermost region of the nanopattern (scan size of 500 nm).

Figure 3a shows that there were 28 features after the first deposition and Figure 3b shows that there were 60 after the second. All the particles deposited in the first step remained after the second deposition. To help visualize this observation, we generated a map showing the position of the particles after the first (1) and second (2) depositions. Several remarkable observations can be derived from these images. First, the deposition time is a parameter that controls the number of particles on the pattern. Second, as long as there is free space on the pattern the particles tend to be placed separately. Figure 3d shows the pattern after a deposition time lasting 4 min (1 + 1 + 1 + 1 min). Here the patterned surface showed a surface coverage of 70 %, close to saturation (see inset in Fig. 3d). The packing of the molecules increased to an average separation of 35 nm (see inset). For long deposition times we also observed a few SMMs located outside but quite close

ADVANCED MATERIALS

to the patterned area (ca. 200 nm); these Mn_{12}bet molecules followed the contours of the patterned stripe.

To ensure that the integrity of the molecules was preserved after deposition, bare and APTES-functionalized silicon wafers were exposed to a 1 μM Mn_{12}bet solution for 10 min. The resulting surfaces were then studied (See Supporting Information) by using X-ray photoelectron spectroscopy (XPS) and time-of-flight secondary ion mass spectrometry (ToF-SIMS; see the Supporting Information for spectra). XPS provided evidence for all the elements expected to be present in the grafted layers with binding energies in good agreement with the expected bonding states. C 1s and Mn 2p (Fig. 4) signals compared well with the data obtained for a single crystal of Mn_{12}bet, whereas the O 1s spectrum was dominated by the presence of a strong Si–O signal originating from the substrate. Analysis of the deposited molecules was also carried out by using ToF-SIMS. Again, the data showed a good match with the spectrum of a Mn_{12}bet crystal. Several characteristic fragments of the polycationic SMMs were detected in all the samples (Table 1). The experimental data clearly indicated that the integrity of the molecules was maintained after the deposition process.

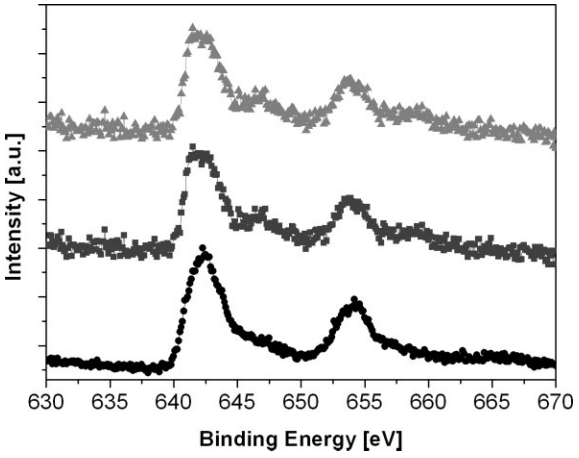

Figure 4. Core-level Mn 2p XPS spectra of Mn_{12}bet deposited onto bare (triangles) and APTES-modified (squares) silicon substrates. The spectrum of a Mn_{12}bet crystal is shown for comparison (circles).

The above results emphasize the possibility of fabricating molecule-based low-dimensional structures by merging bottom-up (the electrostatic interaction between the molecules and the trapped charges) and top-down approaches (the fabrication of the local oxide patterns). These results are general because they can be applied to both charged molecules and noncharged (albeit polarizable) molecules. We applied this process to the nanoscale positioning of very small nanoparticles, in particular SMMs. The accuracy of the positioning is dictated by the size of the lithography. The method could also be applied to generate periodic arrays of SMMs. The present process is scalable, allows multiple processing, and operates with liquid solution. It opens a new avenue for manipulating molecules with nanoscale accuracy in order to incorporate them into technological processes.

Table 1. The characteristic peaks in the ToF-SIMS spectrum (positive mode) of Mn_{12}bet.

m/z	Peak assignment
55	Mn^+
77	$(HO)_2C–CH_2–NH_3^+$
91	$(HO)_2C–CH_2–NH_2(CH_3)^+$
103	$HO_2C–CH_2–N(CH_3)_2^+$
105	$(HO)_2C–CH_2–NH(CH_3)_2^+$
107	$Mn(H_2O)(OH)_2^+$
115	$Mn–O_2CH–CH_3^+$
117	$O_2C–CH_2–N(CH_3)_3^+$
129	$Mn–O_2C–CH_2–NH_2^+$
141	$Mn_2O_2^+$
191	$(HO)_2Mn–O_2C–CH_2–N(CH_3)_2^+$

Experimental

Mn_{12}Ac [35] and Mn_{12}bet [26c] were synthesized according to published procedures. Solvents used were of analytical grade. Chemicals were purchased from Aldrich and used as received. Milli-Q grade water was used. Silicon wafers (p-type Si (100) with a resistivity 10 Ω cm ≤ ρ ≤ 12 Ω cm) were cleaned by using sonication in a H_2O_2/NH_4OH/H_2O (1:1:2) mixture and rinsed with water (three times). They were then dried under nitrogen. To prepare APTES monolayers, the silicon wafer was immersed for 40 min at room temperature in a 1 mM ethanolic solution of APTES. Then it was rinsed with ethanol and dried under nitrogen.

AFM experiments were carried out with an amplitude-modulation atomic force microscope (Digital Instruments, Nano Scope III) operated in the low-amplitude mode (noncontact or attractive regime) and with additional circuits to apply voltage pulses. Noncontact AFM nanolithography was performed with doped n-type silicon cantilevers (Nanosensors, Germany). The force constant k and resonance frequency ν_0 were about 42 N m^{-1} and 320 kHz, respectively. The cantilever was excited at its resonance frequency.

XPS measurements were performed at CACTI (University of Vigo) in a VG Escalab 250 iXL ESCA instrument using monochromatic Al Kα radiation ($h\nu$ = 1486.92 eV; h = Planck's constant). Photoelectrons were collected from a takeoff angle of 90° relative to the sample surface. Measurements were carried out in constant analyzer energy (CAE) mode with a 100 eV pass energy for survey spectra and 20 eV pass energy for high-resolution spectra. Charge referencing was performed by setting the lower binding energy C 1s peak to 285.0 eV.

ToF-SIMS measurements were performed at CACTI (University of Vigo) in a ToF-SIMS IV (Ion-Tof GmbH) surface analyzer at 10^{-10} mbar (1 mbar = 100 Pa) equipped with a liquid Ga-ion source operating at 25 keV in the low-current mode (0.5 pA). The Ga^+-ion beam was rastered over a 500 μm × 500 μm surface and the total ion dose for each analysis was 3×10^{11} ions cm^{-2}.

Received: September 2, 2006
Revised: October 19, 2006

[1] N. Stutzmann, R. H. Friend, H. Sirringhaus, *Science* **2003**, *299*, 1881.
[2] M. D. Austin, S. Y. Chou, *Appl. Phys. Lett.* **2002**, *81*, 4431.
[3] J. A. Rogers, Z. Bao, A. Makhija, P. Braun, *Adv. Mater.* **1999**, *11*, 741.
[4] F. Dinelli, M. Murgia, M. Cavallini, P. Levy, F. Biscarini, D. M. De Leeuw, *Phys. Rev. Lett.* **2004**, *92*, 116 802.

[5] *Alternative Lithography* (Ed: C. M. Sotomayor Torres), Kluwer Academic/Plenum, New York **2003**.
[6] C. R. Barry, J. Gu, H. O. Jacobs, *Nano Lett.* **2005**, *5*, 2078.
[7] P. Mesquida, A. Stemmer, *Adv. Mater.* **2001**, *13*, 1395.
[8] E. Braun, Y. Eichen, U. Sivan, G. Benyoseph, *Nature* **1998**, *391*, 775.
[9] D. Li, G. Ouyang, J. T. McCann, Y. Xia, *Nano Lett.* **2005**, *5*, 913.
[10] R. Garcia, M. Tello, J. F. Moulin, F. Biscarini, *Nano Lett.* **2004**, *4*, 1115.
[11] a) R. Maoz, E. Frydman, S. R. Cohen, J. Sagiv, *Adv. Mater.* **2000**, *12*, 725. b) S. Hoeppener, R. Maoz, J. Sagiv, *Adv. Mater.* **2006**, *18*, 1286.
[12] a) T. Yoshinobu, J. Suzuki, H. Kurooka, W. C. Moon, H. Iwasaki, *Electrochim. Acta* **2003**, *48*, 3131. b) Q. Li, J. Zheng, Z. Liu, *Langmuir* **2003**, *19*, 166.
[13] S. Magdassi, M. Ben Moshe, *Langmuir* **2003**, *19*, 939.
[14] R. Sessoli, D. Gatteschi, A. Caneschi, M. A. Novak, *Nature* **1993**, *365*, 141.
[15] J. R. Friedman, M. P. Sarachik, J. Tejada, R. Ziolo, *Phys. Rev. Lett.* **1996**, *76*, 3830.
[16] H. J. Eppley, H. L. Tsai, N. de Vries, K. Folting, G. Christou, D. N. Hendrickson, *J. Am. Chem. Soc.* **1995**, *117*, 301.
[17] L. Thomas, F. Lionti, R. Ballou, D. Gatteschi, R. Sessoli, B. Barbara, *Nature* **1996**, *383*, 145.
[18] E. M. Chudnovsky, *Nature* **1996**, *274*, 938.
[19] J. Means, V. Meenakshi, R. V. A. Srivastava, W. Teizer, A. A. Kolomenskii, H. A. Schuessler, H. Zhao, K. R. Dunbar, *J. Magn. Magn. Mater.* **2004**, *284*, 215.
[20] M. Cavallini, F. Biscarini, J. Gomez-Segura, D. Ruiz, J. Veciana, *Nano Lett.* **2003**, *3*, 1527.
[21] a) D. Ruiz-Molina, M. Mas-Torrent, J. Gómez, A. I. Balana, N. Domingo, J. Tejada, M. T. Martínez, C. Rovira, J. Veciana, *Adv. Mater.* **2003**, *15*, 42. b) M. Cavallini, J. Gómez-Segura, D. Ruiz-Molina, M. Massi, C. Albonetti, C. Rovira, J. Veciana, F. Biscarini, *Angew. Chem. Int. Ed.* **2005**, *44*, 888.
[22] a) J. S. Steckel, N. S. Persky, C. R. Martinez, C. L. Barnes, E. A. Fry, J. Kulkarni, J. D. Burgess, R. B. Pacheco, S. L. Stoll, *Nano Lett.* **2004**, *4*, 399. b) A. Nait Abdi, J. P. Bucher, P. Rabu, O. Toulemonde, M. Drillon, P. Gerbier, *J. Appl. Phys.* **2004**, *95*, 7345. c) G. G. Condorelli, A. Motta, I. L. Fragalà, F. Giannazzo, V. Raineri, A. Caneschi, D. Gatteschi, *Angew. Chem. Int. Ed.* **2004**, *43*, 4081. d) B. Fleury, L. Catala, V. Huc, C. David, W. Z. Zhong, P. Jegou, L. Baraton, S. Palacin, P.-A. Albouy, T. Mallah, *Chem. Commun.* **2005**, 2020.
[23] A. Naitabdi, J. P. Bucher, P. Gerbier, P. Rabu, M. Drillon, *Adv. Mater.* **2005**, *17*, 1612.
[24] A. Cornia, A. C. Fabretti, M. Pacchioni, L. Zobbi, D. Bonacchi, A. Caneschi, D. Gatteschi, R. Biagi, U. Del Pennino, V. De Renzi, L. Gurevich, H. S. J. van der Zant, *Angew. Chem. Int. Ed.* **2003**, *42*, 1645.
[25] M. Mannini, D. Bonacchi, L. Zobbi, F. M. Piras, E. A. Speets, A. Caneschi, A. Cornia, A. Magnani, B. J. Ravoo, D. N. Reinhoudt, R. Sessoli, D. Gatteschi, *Nano Lett.* **2005**, *5*, 1435.
[26] a) E. Coronado, M. Feliz, A. Forment-Aliaga, C. J. Gómez-García, R. Llusar, F. M. Romero, *Inorg. Chem.* **2001**, *40*, 6084. b) A. Forment-Aliaga, E. Coronado, M. Feliz, A. Gaita-Ariño, R. Llusar, F. M. Romero, *Inorg. Chem.* **2003**, *42*, 8019. c) E. Coronado, A. Forment-Aliaga, A. Gaita-Ariño, C. Giménez-Saiz, F. M. Romero, W. Wernsdorfer, *Angew. Chem. Int. Ed.* **2004**, *43*, 6152.
[27] E. Coronado, A. Forment-Aliaga, F. M. Romero, V. Corradini, R. Biagi, V. De Renzi, A. Gambardella, U. del Pennino, *Inorg. Chem.* **2005**, *44*, 7693.
[28] L. Pellegrino, I. Pallecchi, D. Marre, E. Bellingeri, A. S. Siri, *Appl. Phys. Lett.* **2002**, *81*, 3849.
[29] C. F. Chen, S. D. Tzeng, H. Y. Chen, S. Gwo, *Opt. Lett.* **2005**, *30*, 652.
[30] M. Villarroya, F. Perez-Murano, C. Martín, Z. Davis, A. Boisen, J. Esteve, E. Figueras, J. Montserrat, N. Varonil, *Nanotechnology* **2004**, *15*, 771.
[31] a) M. Tello, R. Garcia, *Appl. Phys. Lett.* **2001**, *79*, 424. b) Instrumentation and nanopatterning process are similar to the one described below but using water menisci: M. Tello, R. Garcia, J. A. Martín-Gago, N. F. Martinez, M. S. Martin-Gonzalez, L. Aballe, A. Baranov, L. Gregoratti, *Adv. Mater.* **2005**, *17*, 1480.
[32] R. Garcia, J. Tamayo, A. San Paulo, *Surf. Interface Anal.* **1999**, *27*, 312.
[33] J. Gómez-Segura, O. Kazakova, J. Davies, P. Josephs-Franks, J. Veciana, D. Ruiz-Molina, *Chem. Commun.* **2005**, 5615.
[34] a) J. Dagata, F. Perez-Murano, C. Martin, H. Kuramochi, H. Yokoama, *J. Appl. Phys.* **2004**, *96*, 2386. b) S. Gwo, personal communication.
[35] T. Lys, *Acta Crystallogr. B* **1980**, *36*, 2042.